NANO LETTERS

Letter

pubs.acs.org/NanoLett

Engineering Topological Surface States of Cr-Doped Bi_2Se_3 Films by Spin Reorientation and Electric Field

Jeongwoo Kim,[†] Seung-Hoon Jhi,[‡] and Ruqian Wu*[,†]

[†]Department of Physics and Astronomy, University of California, Irvine, California 92697, United States

[‡]Department of Physics, Pohang University of Science and Technology, Pohang 790-784, Republic of Korea

Supporting Information

ABSTRACT: The tailoring of topological surface states in topological insulators is essential for device applications and for exploring new topological phase. Here, we propose a practical way to induce the quantum anomalous Hall phase and unusual metal−insulator transitions in Cr-doped Bi_2Se_3 films based on the model Hamiltonian and first-principles calculations. Using the combination of in-plane and plane-normal components of the spin along with external electric fields, we demonstrate that the topological state and band structures of topological insulating films exhibit rich features such as the shift of Dirac cones and the opening of nontrivial band gaps. We also show that the in-plane magnetization leads to significant suppression of inter-TSS scattering in Cr-doped Bi_2Se_3. Our work provides new strategies to obtain the desired electronic structures for the device, complementary to the efforts of an extensive material search.

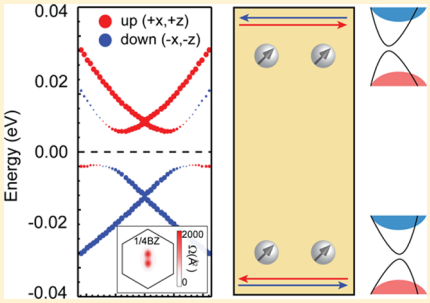

KEYWORDS: *Dirac cone engineering, topological surface state, spin reorientation, quantum anomalous Hall phase*

The topological nature of materials has become a key physical property for active interdisciplinary research as related emergent quantum phenomena are promising for innovative applications.[1−4] By breaking the time-reversal symmetry of topological insulators (TIs) with magnetic dopants, these materials may exhibit the quantized Hall resistance without a magnetic field, known as the quantum anomalous Hall effect (QAHE), which may arise from the exchange and spin orbit coupling (SOC) interactions among electrons.[5] Although QAHE has been successfully observed in Cr- or V-doped $(Bi,Sb)_2Te_3$,[6−8] the requirement of an ultralow temperature [down to milli-Kelvin, primarily due to small band gaps of their topological surfaces states (TSSs)] imposes a harsh limit for the exploitation of this important quantum phenomenon. Many approaches such as thickness variation,[9−11] interfacial proximity effect,[12,13] large Rashba SOC,[14] and magnetic doping by rare earth elements,[15] have been explored to increase the critical temperature of the QAHE, but little progress has been made. This inspires us to perform systematic analyses and simulations for the engineering of band structures of magnetic TIs with a variety of factors, particularly through magnetic reorientation, intersurface coupling, and external electric field in the ultrathin regime. Using Cr-doped Bi_2Se_3 as the prototype, we demonstrated that the critical temperature of the quantum anomalous Hall phase can be tuned by turning the direction of magnetization or by using combination of in-plane and out-of-plane magnetization in samples. When the Cr-doped Bi_2Se_3 film is thinner than 4 quintuple layers (QL), the topological gap can be increased through the coupling of TSSs of the top and bottom surfaces and, furthermore, can be manipulated by applying an electric field. These findings suggest new approaches for Dirac cone engineering that are needed for design of novel spintronic materials.

The TSSs of magnetic TIs can be reasonably described by an effective Hamiltonian as[16−18]

$$H = H_{\mathrm{TSS}} + H_{\mathrm{mag}} + H_{\mathrm{coupling}} \tag{1}$$

$$H_{\mathrm{TSS}} = \sum_{ij\alpha\beta} \tau_{ij}\hbar v(k_x\sigma^y_{\alpha\beta} - k_y\sigma^x_{\alpha\beta})c^\dagger_{ik\alpha}c_{jk\beta} \tag{2}$$

$$H_{\mathrm{mag}} = \sum_{i\alpha\beta} \varepsilon_{\mathrm{d}}(\hat{M}\cdot\vec{\sigma})_{\alpha\beta}d^\dagger_{i\alpha}d_{i\beta} + \sum_{i\alpha} V(d^\dagger_{i\alpha}c_{ik\alpha} + \mathrm{hc}) \tag{3}$$

$$H_{\mathrm{coupling}} = \sum_{i\alpha} t_{\alpha\beta}(c^\dagger_{ik\alpha}c_{i',k\beta} + \mathrm{hc}) \tag{4}$$

where $c_{ik\alpha}$ and $d_{i\alpha}$ are the operators for the surface Dirac Fermion and magnetic electrons, v the Fermi velocity, α, β the spin indices, i, j the site index for two different surfaces, ε_{d} the on-site energy of d-orbitals, $\vec{\sigma}$ the Pauli matrices (the helicity of Dirac Fermions τ is identical to σ_z), $\hat{M}$ the direction of local magnetic moments, V the hybridization between Dirac Fermions and magnetic impurities, and $t_{\alpha\beta}$ represents the coupling between TSSs across the film.

Based on this model, it is obvious that the band structure of magnetic TIs can be tuned by rotating the direction of magnetization. Although it is generally accepted that magnetic moments of Cr or V dopants typically prefer to align along the

Received: August 15, 2016
Revised: September 23, 2016

DOI: 10.1021/acs.nanolett.6b03439
Nano Lett. XXXX, XXX, XXX−XXX

surface normal,[6,7] magnetic reorientation may easily occur since the magnetic anisotropy energy of Cr-doped Bi_2Se_3 (2.2%) is rather small (0.2 meV or 1.1 T according to our calculations).[19] Furthermore, it was proposed that the critical temperature of QAHE could be higher in ferromagnetic insulator (FI)-TI heterostructures, using the proximity effect and high Curie temperature of FI.[12,13] Unlike the conventional current-field alignment for the Hall effect, most FIs such as EuO, EuS, and GdN have in-plane magnetization due to their magnetic anisotropy,[20] and magnetic moments of interfacial atoms can be canted. Therefore, it is imperative to establish theory for how to produce and control the QAHE in the in-plane geometry and how TSSs and the quantum spin Hall effect respond to spin reorientation, which is one of the most important degrees of freedom for magnetic materials. Another tactic to tune the band structure of TSSs is through the remaining coupling between two surfaces across the TI films. Typically, $H_{coupling}$ is negligible when TI is thicker than 5 QL,[21] but it should become appreciable in thin TI films.

To demonstrate the possibility of band engineering through spin reorientation and $H_{coupling}$, density functional theory (DFT) calculations are performed using the projected augmented plane-wave method[22,23] as implemented in the Vienna ab initio simulation package (VASP).[24] We use the Cr-doped Bi_2Se_3 surface as our model system and simulate it with 2- to 5-QL slabs, along with a vacuum of 20 Å. To mimic the case with low concentration of Cr, we use a $(3 \times 3 \times 1)$ supercell expanded in the lateral plane, with one Cr dopant substituting an atom in the second Bi layer from the surface. The generalized gradient approximation is used for the description of exchange-correlation interaction of electrons.[25] The SOC is included in the self-consistent calculations. The energy cutoff for the plane-wave expansion is chosen to be 500 eV. We employ $3 \times 3 \times 1$ **k**-point grid to sample the two-dimensional Brillouin zone. Atomic relaxation is carried out until the change of the total energy becomes less than 0.1 meV. To treat the long-range dispersion force, we invoke the van der Waals correction as suggested by Tkatchenko and Scheffler (TSDF).[26]

To characterize the topological feature, the Chern numbers are directly calculated from the Berry curvature $\Omega(\mathbf{k})$, which is evaluated as follows,[2,27]

$$\Omega(\mathbf{k}) = -2\mathrm{Im}\sum_{n}\sum_{n'\neq n} f_n \frac{\langle\psi_{n\mathbf{k}}|v_x|\psi_{n'\mathbf{k}}\rangle\langle\psi_{n'\mathbf{k}}|v_y|\psi_{n\mathbf{k}}\rangle}{(\varepsilon_{n'\mathbf{k}} - \varepsilon_{n\mathbf{k}})^2} \quad (5)$$

where n is the band index, f_n is the Fermi–Dirac distribution function, $v_{x(y)}$ is the velocity operator, and $\psi_{n\mathbf{k}}$ and $\varepsilon_{n\mathbf{k}}$ are the Bloch wave function and energy of the n-th band at a **k** point, respectively. The Berry curvature is estimated from the maximally localized Wannier function using the WANNIER90 package.[28]

As illustrated in Figure 1a, the perpendicular magnetic impurities give rise to a mass gap ($M\sigma_z$) of TSSs, whereas the in-plane magnetic impurities (e.g., along the x-axis) cause a shift of the Dirac point by $M\sigma_x$ in the momentum space. This is confirmed by DFT results for 5-QL Cr-doped Bi_2Se_3 (2.2%) as shown in Figure 1b. The TSS is shifted by in-plane magnetization (x-axis) away from Γ point but retains its gapless Dirac-cone shape (red lines), in contrast to the gap opening induced by the perpendicular magnetization. Note that the distinct effect of magnetic orientation on TSS is general, independent of the type and location of magnetic impurities.

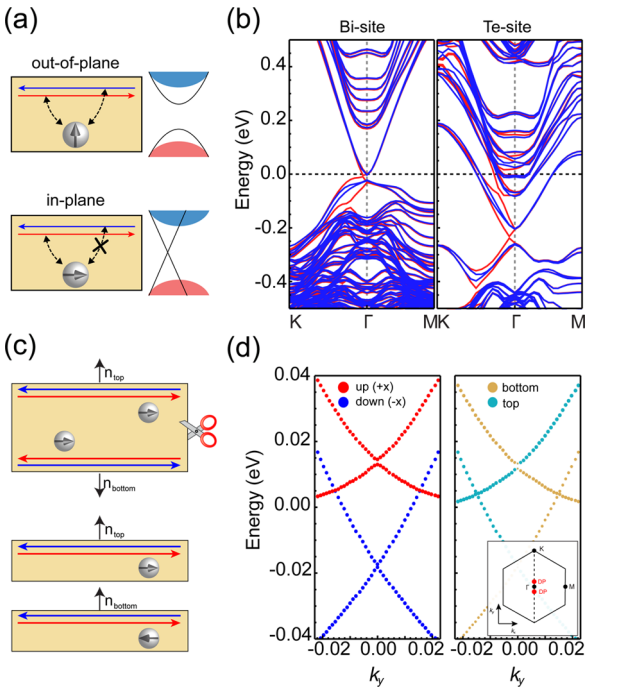

Figure 1. (a) Schematic drawings of Cr-doped Bi_2Se_3 for different spin directions of Cr dopants (gray arrows). Dotted lines represent the interaction between spin-polarized TSSs (red and blue arrows) and Cr dopants. (b) Calculated band structures of 5-QL Bi_2Se_3 with Cr doping on Bi-sites (left panel) and Se-sites (right panel), respectively. Red (blue) lines for Cr-doped Bi_2Se_3 with magnetization along the x-axis (z-axis). (c) Schematic drawing of Cr-doped Bi_2Se_3 with the in-plane magnetization. TSSs on each surface experience the opposite magnetic moment due to their different helicities. Red and blue arrows represent a pair of TSS, and localized Cr spins are denoted by gray arrows. (d) Spin-projected and site-projected band structures of 5-QL Cr-doped Bi_2Se_3 with the in-plane magnetization. The x-components (namely, spin-up and spin-down parts in the left panel) and the contributions of the top and bottom surfaces (right panel) are given in different colors. Inset is the first Brillouin zone of Cr-doped Bi_2Se_3 slab structure and the high symmetry points. Red dots are positions of the shifted Dirac points.

For example, the main feature of electronic structure is essentially the same when Fe or Mo is used in lieu of Cr (Figure S1). We also tested two substitutional sites, Bi and Te sites, and a sharp linear dispersion near Γ point is clearly observed in both cases (Figure 1b).

Another interesting thing to note is that the top and bottom TSSs move in opposite directions and TSSs with different spin helicity are split in the momentum space, in analogous to Weyl semimetals (Figure 1c,d). As illustrated in Figure 1c, top and bottom surfaces have different spin helicities, and thus the effective magnetic field should be different (Figure 1d). The splitting of TSSs is also robust against the surface deformation such as O_2 adsorption (Figure S2). Therefore, if we control the direction of magnetization of top and bottom surfaces separately using the proximity effect of heterostructure, external electric or magnetic fields (Figure S3), the separation of Dirac cone can be adjusted by the relative angles between the top and bottom magnetization. We expect intriguing electronic structures such as van Hove singularity of twisted-bilayer graphene to be observed in TIs.[29,30] Furthermore, the position of the Dirac cone can be changed by the rotation of spins in the xy-plane (Figure S4).

DOI: 10.1021/acs.nanolett.6b03439
Nano Lett. XXXX, XXX, XXX−XXX

With the control of spin direction, the Dirac cone engineering can be achieved without compromising its exotic nature. Because of the very small anisotropy energy of Cr in Bi_2Se_3, the rapid quenching in external magnetic field may freeze local spins along the desired direction. For the magnetization along 45° in the *xz*-plane (or the combination of in-plane and out-of-plane magnetization) as illustrated in Figure 2a, top and bottom TSSs are still separated in momentum by in-plane magnetization, along with the gap opening caused by out-of-plane magnetization (Figure 2b). The spin-projected band structure clearly shows the band inversion of two different spin states, which is a convincing signature of the nontrivial topology. Unlike the traditional QAHE geometry in which both the nontrivial band topology and a band gap are driven solely by the perpendicular magnetization, for the canted spin geometry, the role of out-of-plane magnetization is just to produce a gap and thus it does not affect the band topology. Through Berry curvature calculations, we find nonzero Berry curvature near the Γ point, and the integration of the Berry curvature over the first Brillouin zone shows that, as anticipated, QAH phase can be realized by the tilted magnetic moment with a Chern number of 1 (Figure 2b). We suggest that the Cr-doped TI sandwiched by FIs can be a pragmatic platform to realize QAHE with the tilted magnetic moments. Since FI is a good source of the in-plane magnetic field in terms of the uniformity and tenability (Figure S4), the combination with Cr atoms having the perpendicular magnetic moment is likely to display the intriguing topological feature predicted in this work. This is interesting since Cr-doped TIs can have the QAH phase with an integer Chern number by the interplay of in-plane and out-of-plane magnetization without satisfying the certain synthetic conditions.

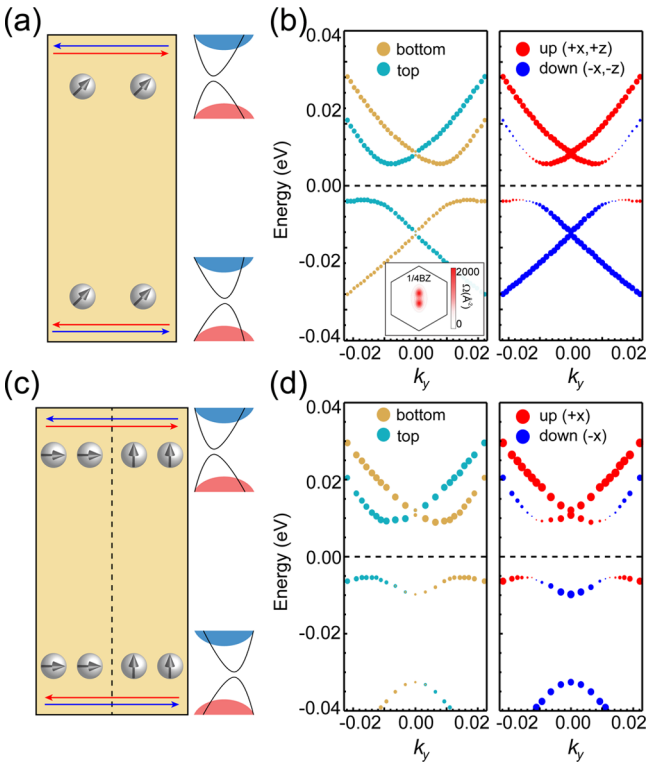

Figure 2. (a) Schematic drawing and (b) site-projected and spin-projected band structures of 5-QL Cr-doped Bi_2Se_3 with magnetization pointing to 45° in the *xz*-plane. The inset is the calculated Berry curvature of the valence band for the combined magnetization with the Brillouin zone scaled down to one-fourth of its original size. (c) Schematic drawing and (d) site-projected and spin-projected band structures of 4-QL Cr-doped Bi_2Se_3 with the alternating in-plane and out-of-plane magnetic moments in the lateral direction. The size of the magnetic domain is 17 Å. In parts a and c, red and blue arrows represent a pair of TSSs and the gray arrows the directions of Cr spins.

We also find that, without direct spin rotation to a certain angle, QAH phase can be achieved by the mixture of the in-plane and the out-of-plane magnetic domains. In other words, the alternating in-plane and out-of-plane magnetization in the lateral plane is equivalent to directly tilting the localized spins. TSSs are widespread in the surfaces, and the net sum of magnetic components in different regions acts as the effective magnetic moment acting on TSSs (Figure S5). Even if two magnetic domains are spatially separated as illustrated in Figure 2c, TSSs take their averaged effect, and the electronic structures are almost the same as that obtained by the spin rotation. Therefore, we can easily modify the surface electronic structure and the band topology of TIs by mixing different ferromagnetic materials at the nanometer scale.

Based on the resilient topological nature resulting from the spin reorientation, we may further modify the electronic structure of TSSs through the $t_{\alpha\beta}$ term in eq 4, by changing the thickness of TI and by applying electric fields. In Figure 3, the variation of TSS upon decreasing the thickness of Cr-doped Bi_2Se_3 while keeping in-plane magnetization is displayed. The shifted Dirac cones remain up to 4 QL, but the linear dispersion disappears, and the system becomes insulating from 3 QL

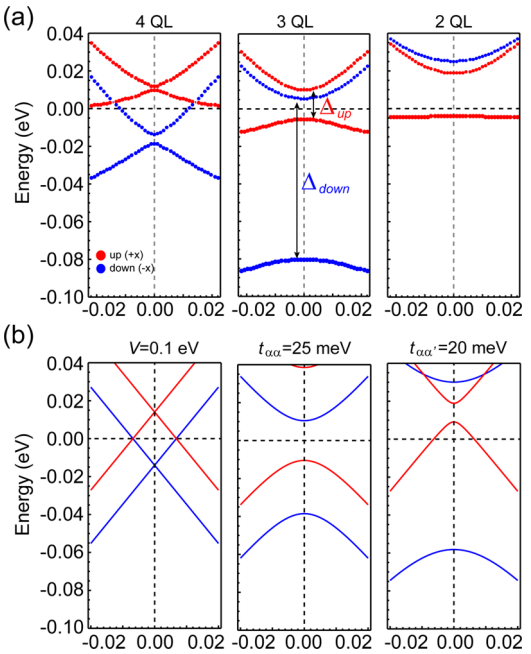

Figure 3. (a) Calculated band structures of Cr-doped Bi_2Se_3 from 4 QL to 2 QL (from left to right panels). Blue (red) dots means spin-up (-down) component along the *x*-axis. The mass gap of up-states Δ_{up} and down-states Δ_{down} induced by the interaction between TSSs increase as the film thickness decreases. (b) From left to right, band structures from the model Hamiltonian for the geometry of in-plane magnetization with V = 0.1 eV, $t_{\alpha\alpha}$ = $t_{\alpha\alpha'}$ = 0 meV; V = 0.1 eV, $t_{\alpha\alpha}$= 25 meV, $t_{\alpha\alpha'}$ = 0 meV; and V = 0.1 eV, $t_{\alpha\alpha}$= 25 meV, $t_{\alpha\alpha'}$ = 20 meV, respectively. Red (blue) lines represent spin-up (down) component along the *x*-axis.

DOI: 10.1021/acs.nanolett.6b03439
Nano Lett. XXXX, XXX, XXX−XXX

(Figure 3a). The energy splitting of spin-down states (Δ_{down}) reaches up to about 80 meV in 3 QL, which is far greater than 20 meV splitting between spin-up states (Δ_{up}). For 2QL, the order of conduction bands is different from that of 3 QL, and the gap is reduced to 23 meV, much less than the pure Bi_2Se_3 band gap (132 meV).

The alternation of band structures with the change of thickness can be well-reproduced using the model Hamiltonian in eq 1. As shown in Figure 3b, the inclusion of nonspin flipping coupling ($t_{\alpha\alpha} = t_{\alpha'\alpha'} = 25$ meV) between the surfaces leads to the hybridization of top and bottom TSSs and makes Δ_{up} and Δ_{down} equal to each other. By including the spin flipping coupling ($t_{\alpha\alpha'} = t_{\alpha'\alpha} = 20$ meV), we obtain the inverted band order and the spin-selective energy splitting in DFT results in Figure 3a. Through unitary transformation, the inter-TSS coupling in the spin-up ($+x$ direction) channel corresponds to $t_{\alpha\alpha} - t_{\alpha\alpha'}$, whereas it changes to $t_{\alpha\alpha} + t_{\alpha\alpha'}$ in the spin-down ($-x$ direction) channel. In other words, the backscattering of the spin channels parallel to the magnetization direction is suppressed by in-plane magnetization, whereas the scattering between the antiparallel spin channels is enhanced. The difference in the scattering rate between the spin-up and spin-down channels gives rise to the spin polarization of the states near the Fermi level. The nonspin flipping coupling can be tuned by the thickness of TI and the spin flipping coupling by the magnetic impurity concentration (or the in-plane magnetic fields). Therefore, in-plane magnetization can be utilized as a new way to realize spin-polarized TSSs and to control its band gap in ultrathin TI films.

Another easy way to modify electronic structure of materials is to apply an external electric field through gate voltage. Here, we use 2 QL Bi_2Se_3 with in-plane magnetization as a model system to examine the interplay between the inter-TSS coupling and the electric field. As mentioned before, the hybridization between two surface states becomes important for TI films less than 4 QL (Figure 3a). The presence of an external electric field adjusts the potentials of the top and bottom surfaces and subsequently the energies of two TSSs. As a result, dramatic changes in band structures can be produced by a small field, as shown in Figure 4a. The site-projected band structure clearly shows that the bottom TSS moves downward and the top TSS upward when an electric field is applied (Figure 4b). Interestingly, spin-down states have an obvious gap, whereas spin-up channel becomes metallic. This means that Cr-doped Bi_2Se_3 films can be easily tuned between the half-metallic and insulating states by adjusting gate voltages. We note that this phase transition driven by electric fields occurs in 3 QL layers as well (Figure S7). Our results suggest the possibility of utilizing the phase transition as a spin device controlled by electric fields.

In summary, we proposed a new way of manipulating TSSs to realize the QAH phase and a half-metallic phase in Cr-doped Bi_2Se_3 films through first-principles calculations. The shift of Dirac cones in the reciprocal space can be achieved by the spin reorientation, and the QAH phase is possible in TI with the coexistence of in-plane and out-of-plane magnetization. The backscattering of TSSs between different surface states is significantly reduced in the geometry of in-plane magnetization even when the thickness of Cr-doped Bi_2Se_3 is less than 4 QL, and these TSSs may be further tuned between half-metallic and insulating states by applying an electric field. Complementary to vast search of exotic materials, our new approach for Dirac cone engineering through the control of orientation of magnetization and intersurface coupling is suitable for operations in spintronic devices.

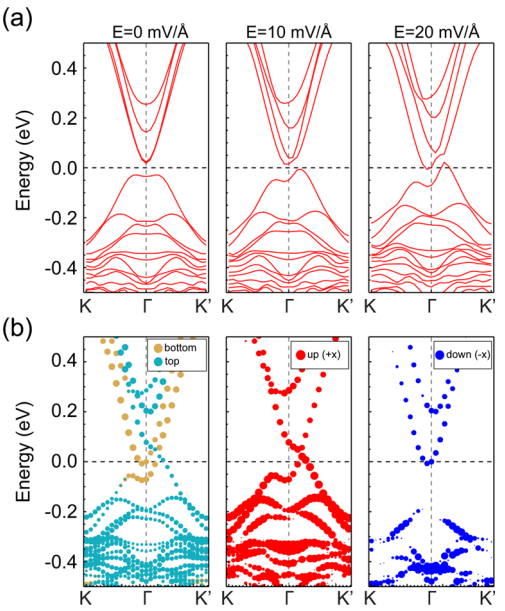

Figure 4. (a) Evolution of electronic structure of 2 QL Cr-doped Bi_2Se_3 upon applying electric fields. (b) Site-projected and spin-projected band structures of Cr-doped Bi_2Se_3 (2 QL) in an external field of 20 mV/Å. The contribution of top and bottom surfaces (left panel) and the spin x-component with up (middle panel) and down (right panel).

■ ASSOCIATED CONTENT

Supporting Information

The Supporting Information is available free of charge on the ACS Publications website at DOI: 10.1021/acs.nanolett.6b03439.

Topological surface states of Fe-doped and Mo-doped Bi_2Se_3, the effect of O_2 adsorption on Cr-doped Bi_2Se_3, the proximity effect of in-plane magnetization on topological surfaces states, the manipulation of the Dirac cone by the control of magnetization direction, the effects of the in-plane and perpendicular magnetic domains on TSS, and the evolution of band structure upon applying E-fields in 3 QL (PDF)

■ AUTHOR INFORMATION

Corresponding Author

*E-mail: wur@uci.edu.

Notes

The authors declare no competing financial interest.

■ ACKNOWLEDGMENTS

Work was supported as part of the SHINES, an Energy Frontier Research Center funded by the U.S. Department of Energy, Office of Science, Basic Energy Sciences, under Grant No. SC0012670. Calculations were performed on parallel computers at NERSC supercomputer centers. S.H.J. was supported by the National Research Foundation of Korea through SRC program (Grant No. 2011-0030046).

DOI: 10.1021/acs.nanolett.6b03439
Nano Lett. XXXX, XXX, XXX−XXX

REFERENCES

(1) Klitzing, K. v.; Dorda, G.; Pepper, M. *Phys. Rev. Lett.* **1980**, *45* (6), 494−497.
(2) Thouless, D. J.; Kohmoto, M.; Nightingale, M. P.; den Nijs, M. *Phys. Rev. Lett.* **1982**, *49* (6), 405−408.
(3) Kane, C. L.; Mele, E. J. *Phys. Rev. Lett.* **2005**, *95* (14), 146802.
(4) Bernevig, B. A.; Hughes, T. L.; Zhang, S.-C. *Science* **2006**, *314* (5806), 1757−1761.
(5) Yu, R.; Zhang, W.; Zhang, H.-J.; Zhang, S.-C.; Dai, X.; Fang, Z. *Science* **2010**, *329* (5987), 61−64.
(6) Chang, C.-Z.; Zhang, J.; Feng, X.; Shen, J.; Zhang, Z.; Guo, M.; Li, K.; Ou, Y.; Wei, P.; Wang, L.-L.; Ji, Z.-Q.; Feng, Y.; Ji, S.; Chen, X.; Jia, J.; Dai, X.; Fang, Z.; Zhang, S.-C.; He, K.; Wang, Y.; Lu, L.; Ma, X.-C.; Xue, Q.-K. *Science* **2013**, *340* (6129), 167−170.
(7) Chang, C.-Z.; Zhao, W.; Kim, D. Y.; Zhang, H.; Assaf, B. A.; Heiman, D.; Zhang, S.-C.; Liu, C.; Chan, M. H. W.; Moodera, J. S. *Nat. Mater.* **2015**, *14* (5), 473−477.
(8) Checkelsky, J. G.; Yoshimi, R.; Tsukazaki, A.; Takahashi, K. S.; Kozuka, Y.; Falson, J.; Kawasaki, M.; Tokura, Y. *Nat. Phys.* **2014**, *10*, 731−736.
(9) Kou, X.; Guo, S.-T.; Fan, Y.; Pan, L.; Lang, M.; Jiang, Y.; Shao, Q.; Nie, T.; Murata, K.; Tang, J.; Wang, Y.; He, L.; Lee, T.-K.; Lee, W.-L.; Wang, K. L. *Phys. Rev. Lett.* **2014**, *113* (13), 137201.
(10) Feng, X.; Feng, Y.; Wang, J.; Ou, Y.; Hao, Z.; Liu, C.; Zhang, Z.; Zhang, L.; Lin, C.; Liao, J.; Li, Y.; Wang, L.-L.; Ji, S.-H.; Chen, X.; Ma, X.; Zhang, S.-C.; Wang, Y.; He, K.; Xue, Q.-K. *Adv. Mater.* **2016**, *28* (30), 6386−6390.
(11) Duong, L. Q.; Lin, H.; Tsai, W.-F.; Feng, Y. P. *Phys. Rev. B: Condens. Matter Mater. Phys.* **2015**, *92* (11), 115205.
(12) Li, M.; Chang, C.-Z.; Kirby, B. J.; Jamer, M. E.; Cui, W.; Wu, L.; Wei, P.; Zhu, Y.; Heiman, D.; Li, J.; Moodera, J. S. *Phys. Rev. Lett.* **2015**, *115* (8), 087201.
(13) Liu, W.; He, L.; Xu, Y.; Murata, K.; Onbasli, M. C.; Lang, M.; Maltby, N. J.; Li, S.; Wang, X.; Ross, C. A.; Bencok, P.; van der Laan, G.; Zhang, R.; Wang, K. L. *Nano Lett.* **2015**, *15* (1), 764−769.
(14) Qiao, Z.; Jiang, H.; Li, X.; Yao, Y.; Niu, Q. *Phys. Rev. B: Condens. Matter Mater. Phys.* **2012**, *85* (11), 115439.
(15) Chen, T.; Liu, W.; Zheng, F.; Gao, M.; Pan, X.; van der Laan, G.; Wang, X.; Zhang, Q.; Song, F.; Wang, B.; Wang, B.; Xu, Y.; Wang, G.; Zhang, R. *Adv. Mater.* **2015**, *27* (33), 4823−4829.
(16) Fu, L. *Phys. Rev. Lett.* **2009**, *103* (26), 266801.
(17) Henk, J.; Flieger, M.; Maznichenko, I. V.; Mertig, I.; Ernst, A.; Eremeev, S. V.; Chulkov, E. V. *Phys. Rev. Lett.* **2012**, *109* (7), 076801.
(18) Kim, J.; Jhi, S.-H. *Phys. Rev. B: Condens. Matter Mater. Phys.* **2015**, *92* (10), 104405.
(19) Aramberri, H.; Muñoz, M. C. *Phys. Rev. B: Condens. Matter Mater. Phys.* **2016**, *93* (24), 245401.
(20) Chang, C.-Z.; Li, M. *J. Phys.: Condens. Matter* **2016**, *28* (12), 123002.
(21) Zhang, Y.; He, K.; Chang, C.-Z.; Song, C.-L.; Wang, L.-L.; Chen, X.; Jia, J.-F.; Fang, Z.; Dai, X.; Shan, W.-Y.; Shen, S.-Q.; Niu, Q.; Qi, X.-L.; Zhang, S.-C.; Ma, X.-C.; Xue, Q.-K. *Nat. Phys.* **2010**, *6* (8), 584−588.
(22) Blöchl, P. E. *Phys. Rev. B: Condens. Matter Mater. Phys.* **1994**, *50* (24), 17953−17979.
(23) Kresse, G.; Joubert, D. *Phys. Rev. B: Condens. Matter Mater. Phys.* **1999**, *59* (3), 1758−1775.
(24) Kresse, G.; Hafner, J. *Phys. Rev. B: Condens. Matter Mater. Phys.* **1994**, *49* (20), 14251.
(25) Perdew, J. P.; Burke, K.; Ernzerhof, M. *Phys. Rev. Lett.* **1996**, *77* (18), 3865.
(26) Tkatchenko, A.; Scheffler, M. *Phys. Rev. Lett.* **2009**, *102* (7), 073005.
(27) Yao, Y.; Kleinman, L.; MacDonald, A. H.; Sinova, J.; Jungwirth, T.; Wang, D.-s.; Wang, E.; Niu, Q. *Phys. Rev. Lett.* **2004**, *92* (3), 037204.
(28) Mostofi, A. A.; Yates, J. R.; Lee, Y.-S.; Souza, I.; Vanderbilt, D.; Marzari, N. *Comput. Phys. Commun.* **2008**, *178* (9), 685−699.
(29) Li, G.; Luican, A.; Lopes dos Santos, J. M. B.; Castro Neto, A. H.; Reina, A.; Kong, J.; Andrei, E. Y. *Nat. Phys.* **2009**, *6* (2), 109−113.
(30) Kim, Y.; Herlinger, P.; Moon, P.; Koshino, M.; Taniguchi, T.; Watanabe, K.; Smet, J. H. *Nano Lett.* **2016**, *16* (8), 5053−5059.

DOI: 10.1021/acs.nanolett.6b03439
Nano Lett. XXXX, XXX, XXX−XXX